

0017-9310(94)E0001-B

Mixed convection with flow reversal in the thermal entrance region of horizontal and vertical pipes

M. WANG, T. TSUJI and Y. NAGANO†

Department of Mechanical Engineering, Nagoya Institute of Technology, Nagoya 466, Japan

(Received 30 September 1993 and in final form 9 December 1993)

Abstract—Numerical analyses have been conducted for combined free and forced laminar convection flow at low Péclet numbers in the thermal entrance region of horizontal and vertical pipes. Effects of both buoyancy force and axial conduction on the hydrodynamic and heat transfer characteristics are systematically investigated, and numerical results are extensively presented for velocity and temperature profiles, distributions of the Nusselt number and wall shear stress in both horizontal and vertical pipes. In a horizontal pipe, the secondary flow pattern has already developed at the beginning of heating and a reverse flow occurs near the pipe top as the axial conduction and buoyancy effects become large. Consequently, the local Nusselt number at the pipe top and then the circumferential average Nusselt number decrease with increasing secondary flow. The regime of reverse flow is clearly identified in the $Pe-Ra$ coordinates. In a vertical pipe, flow reversals are observed at the pipe center in the heating case and near the wall in the cooling case at relatively high $|Gr/Re|$. The regime of reverse flow is identified for both heating and cooling cases in the $Pe-|Gr/Re|$ coordinates.

1. INTRODUCTION

COMBINED free and forced convection in the pipe entrance region has many diverse industrial and engineering applications, such as heat exchangers and chemical processes. Because of the practical interest numerous investigations of mixed flows in the pipe entrance region have been conducted analytically and experimentally by various researchers, and great progress has been made in this area during the past 20 years.

Prior to 1980 there were several analytical studies [1–4] on the entrance region of horizontal circular pipes. They used the large Prandtl number assumption which neglected the nonlinear inertia terms in the momentum equations to avoid the complexities arising from the three-dimensionality of flow, and thus the results were consequently available for a limited situation and unsuitable for small and even moderate Prandtl number fluids. Later, numerical analyses without the large Prandtl number assumption were conducted and significant results were obtained by Hishida *et al.* [5] for $Pr = 0.71$ and by Chou and Hwang [6] for $Pr = 0.7, 2$ and 5 . In ref. [6] the axial viscous and conduction terms included in the momentum and thermal energy equations were neglected for ease of computation.

On the other hand, the combined flows in the entrance region of vertical pipes have also been investigated analytically and experimentally by several

researchers. Numerical analyses were performed by Lawrence and Chato [7] and Marner and McMillan [8] with the assumption that the axial diffusions of heat and momentum could be ignored. Calculations taking account of the axial diffusions of heat and momentum were carried out by Zeldin and Schmidt [9] for air flow in an isothermal pipe with Pe of about 250. Kieda *et al.* [10] analyzed upward and downward flows of air and water with temperature-dependence properties and observed flow reversals under both flow conditions. Morton *et al.* [11] focused their attention on a recirculating behavior produced in mixed flows and compared the numerical results with experimental ones for water.

The investigations mentioned above were concerned with mixed convection in the entrance region for relatively high Prandtl number fluids. There have been few investigations of low Prandtl or Péclet number fluids, such as liquid metals which are used in practice as heat transfer media in the nuclear-reactor cooling process and compact heat exchangers. For low Pr fluids the axial conduction plays a pronounced role in flow and heat transfer characteristics, as is well known for pure forced convection in pipes [12–16]. In the present study low Péclet number flows in the thermal entrance regions of horizontal and vertical pipes are systematically analyzed in view of the simultaneous effects of free convection and axial conduction. The variation of velocity and thermal fields in the pipe entrance region are extensively investigated and the regime of reverse flow occurrence is clearly identified with the relevant flow parameters.

† To whom correspondence should be addressed.

$$= -\frac{r}{2} \frac{\partial p}{\partial \xi} \frac{d\xi}{dx} + \nabla^2 W - \frac{2}{r} \frac{\partial W}{\partial r} + \frac{W}{r^2} \quad (4)$$

$$\frac{\partial \theta}{\partial \tau} + \frac{1}{r} \left(U \frac{\partial \theta}{\partial r} + \frac{V}{r} \frac{\partial \theta}{\partial \phi} + W \frac{\partial \theta}{\partial \xi} \frac{d\xi}{dx} \right) = \frac{1}{Pr} \nabla^2 \theta, \quad (5)$$

where the Laplacian operator is defined as

$$\nabla^2 = \frac{\partial^2}{\partial r^2} + \frac{1}{r} \frac{\partial}{\partial r} + \frac{1}{r^2} \frac{\partial^2}{\partial \phi^2} + \left(\frac{2}{Re} \right)^2 \left\{ \left(\frac{d\xi}{dx} \right)^2 \frac{\partial^2}{\partial \xi^2} + \frac{d^2 \xi}{dx^2} \frac{\partial}{\partial \xi} \right\}. \quad (6)$$

The dimensionless variables in equations (1)–(6) are chosen as follows:

$$\begin{aligned} \tau &= (\tau' w'_0 / r'_0) (2/Re), & x &= (x' / r'_0) (2/Re) \\ r &= r' / r'_0, & u &= (u' / w'_0) (Re/2) \\ v &= (v' / w'_0) (Re/2), & w &= w' / w'_0 \\ \theta &= (t' - t'_w) / (t'_0 - t'_w), & p &= p' / (\rho w'^2_0 / 2). \end{aligned} \quad (7)$$

Also, the following transformations of the variables are used to ensure numerical stability and to make the axial boundary finite:

$$U = ru, \quad V = rv, \quad W = rw \quad (8)$$

$$\xi = 1/(1 - 30x) - 1 \quad \text{for } -\infty \leq x < 0$$

$$\xi = 1 - 1/(1 + 30x) \quad \text{for } 0 \leq x \leq \infty. \quad (9)$$

The above set of equations is sufficient to obtain solutions for U, V, W, θ and p . For the pressure, however, a more accurate solution can be determined from the Poisson form of the pressure equation, which is derived from the continuity and momentum equations and is expressed as follows:

$$\begin{aligned} \nabla^2 p &= -2 \left(\frac{2}{Re} \right)^2 \left[\frac{1}{r} \left\{ \frac{\partial D}{\partial \tau} + \frac{1}{r} \right. \right. \\ &\times \left(U \frac{\partial D}{\partial r} + \frac{V}{r} \frac{\partial D}{\partial \phi} + W \frac{\partial D}{\partial \xi} \frac{d\xi}{dx} - \frac{UD}{r} \right) \\ &\left. \left. - \nabla^2 D + \frac{2}{r} \frac{\partial D}{\partial r} - \frac{D}{r^2} \right\} \right. \\ &+ Gr \left(\cos \phi \frac{\partial \theta}{\partial r} - \sin \phi \frac{1}{r} \frac{\partial \theta}{\partial \phi} \right) \\ &+ \frac{1}{r^2} \left\{ \left(\frac{\partial U}{\partial r} \right)^2 + \left(\frac{1}{r} \frac{\partial V}{\partial \phi} \right)^2 + \left(\frac{\partial W}{\partial \xi} \frac{d\xi}{dx} \right)^2 \right. \\ &+ \frac{U^2 + V^2}{r^2} + \frac{2}{r} \left(\frac{U}{r} \frac{\partial V}{\partial \phi} - \frac{V}{r} \frac{\partial U}{\partial \phi} \right) \\ &\left. - \frac{\partial}{\partial r} \left(\frac{U^2 + V^2}{r} \right) - \frac{2W}{r} \frac{\partial U}{\partial \xi} \frac{d\xi}{dx} + \frac{2}{r} \frac{\partial U}{\partial \phi} \frac{\partial V}{\partial r} \right] \end{aligned}$$

$$\left. + \frac{2}{r} \frac{\partial W}{\partial \phi} \frac{\partial V}{\partial \xi} \frac{d\xi}{dx} + 2 \frac{\partial U}{\partial \xi} \frac{d\xi}{dx} \frac{\partial W}{\partial r} \right\}, \quad (10)$$

where D , called the dilatation term, is

$$D = \frac{\partial U}{\partial r} + \frac{1}{r} \frac{\partial V}{\partial \phi} + \frac{\partial W}{\partial \xi} \frac{d\xi}{dx}. \quad (11)$$

The dilatation term D is retained in the Poisson equation in order to avoid error accumulation in the iteration, although the continuity equation (1) just states that $D = 0$.

The boundary conditions for equations (1)–(5) and (10) are as follows:

$$\xi = -1, 0 \leq r < 1: \quad U = V = 0$$

$$w = W/r = 2(1 - r^2), \quad \theta = 1$$

$$\left(\frac{\partial p}{\partial \xi} \right) \left(\frac{d\xi}{dx} \right) = -16 \quad (12)$$

$$\xi = 1, 0 \leq r < 1: \quad U = V = 0$$

$$w = W/r = 2(1 - r^2), \quad \theta = 0$$

$$\left(\frac{\partial p}{\partial \xi} \right) \left(\frac{d\xi}{dx} \right) = -16 \quad (13)$$

$$-1 \leq \xi < 0, r = 1: \quad U = V = W = 0, \quad \partial \theta / \partial r = 0$$

$$\frac{\partial p}{\partial r} = 2(2/Re)^2 \left(\partial^2 U / \partial r^2 - \partial U / \partial r - Gr \theta \cos \phi \right) \quad (14)$$

$$0 \leq \xi \leq 1, r = 1: \quad U = V = W = 0, \quad \theta = 0$$

$$\frac{\partial p}{\partial r} = 2(2/Re)^2 \left(\partial^2 U / \partial r^2 - \partial U / \partial r \right) \quad (15)$$

$$-1 \leq \xi \leq 1, 0 \leq r \leq 1, \phi = 0, \pi: \quad V = 0. \quad (16)$$

The pressure varies linearly with the axial distance in the fully developed flow region, as seen from equations (12) and (13). Hence, let the asymptotic pressure solution be P . Then we can write P as

$$P(r, \phi, x) = p + 16x. \quad (17)$$

Using P instead of p , the boundary conditions for P become equal to equations (14) and (15) at the pipe wall, and are written, respectively, at infinite upstream and downstream in equations (12) and (13) as

$$\xi = -1, 0 \leq r < 1: \quad \partial P / \partial \xi = 0$$

$$\xi = 1, 0 \leq r < 1: \quad \partial P / \partial \xi = 0. \quad (18)$$

The finite difference method was employed to numerically solve the above equations. Euler's modified method and the Crank–Nicolson method were used for the time integration. The advection terms in the time-dependent momentum and energy equations were approximated by upwind differencing. The derivative boundary conditions for the pressure P were evaluated by applying Miyakoda's scheme [17]. In order to investigate the low Pr effect systematically, the problems for a wide range of Pr including those of liquid metals such as mercury and sodium were solved with the successive over-relaxation (SOR) method. The ranges of parameters used in the study are $Pe = 0.001$ – 700 and $Ra = 0.05$ – $35\,000$ (consisting of $Pr = 0.00001$ – 7 , $Re = 100$ – 300 and $Gr = 3000$ –

20 000). The calculations were carried out in one-half of the circular region, because of the symmetry about the vertical centerline. The mesh size of $26 \times 27 \times 51$ (r, ϕ, ξ) was used. For the case of $Pr = 0.025$ ($Pe = 2.5$) and $Ra = 500$, where the distortions of velocity and temperature profiles are strongest, a finer mesh size of $51 \times 27 \times 101$ was used in order to confirm the numerical accuracy. There was no significant difference between the results with two mesh sizes. The computations continued with increasing time levels until the steady-state profiles were obtained. The criterion for convergence was $|Q^{n+1} - Q^n| / |Q^n|_{\text{Max}} < 10^{-5}$ ($Q: U, V, W, \text{etc.}$). All problems have been solved on TITAN 3000 and FACOM M-1800/20 systems.

2.2. Vertical pipe

The physical model under consideration is illustrated in Fig. 1(b). The pipe wall is insulated in the upstream region ($x' < 0$) and kept at a constant temperature in the downstream region ($x' \geq 0$), similar to the situation of a horizontal pipe. Numerical analyses are conducted for the fluid heating and cooling with upward flow, in which the fluid flow is axially symmetric and thus becomes two-dimensional. The results obtained from the analyses are applicable to the case of the fluid cooling and heating with downward flow, if the fluid properties are constant. The governing equations of continuity, momentum and energy and the Poisson equation of pressure are represented by those eliminating the terms related to the angle ϕ and the velocity component V in equations (1), (2), (4), (5) and (10), respectively. Then, in the momentum equation in the vertical direction, the buoyancy term $-(2/Re)Gr \cdot r\theta$ is included. Here, the value of Gr is positive for the heating case and negative for the cooling case. Also, in the Poisson equation of pressure, the buoyancy term $2(Gr/Re)(\partial\theta/\partial\xi)(d\xi/dx)$ is added. For the axial distance, the following transformation is used instead of equation (9):

$$\begin{aligned} \xi &= 1/(1-10x) - 1 & \text{for } -\infty \leq x < 0 \\ \xi &= 1 - 1/(1+10x) & \text{for } 0 \leq x \leq \infty. \end{aligned} \quad (19)$$

The boundary conditions are the same as those described by equations (12)–(15) except that the pressure condition in equation (12) is modified by $(\partial p/\partial\xi)(d\xi/dx) = -16 - 4(Gr/Re)$, and the buoyancy term included in equation (14) is eliminated. Using P defined by equation (17), the pressure conditions at infinite upstream and downstream are written as

$$\begin{aligned} \xi &= -1, 0 \leq r < 1: & \partial P/\partial\xi &= -4Gr/Re \\ \xi &= 1, 0 \leq r < 1: & \partial P/\partial\xi &= 0. \end{aligned} \quad (20)$$

Using the same numerical method as for a horizontal pipe, the solutions were obtained for $Pe = 0.7-71$ and $|Gr/Re| = 50-500$ ($Pr = 0.007, 0.025, 0.1, 0.71$, $Re = 50, 100$ and $|Gr| = 5000, 10\,000, 20\,000, 50\,000$). Two mesh sizes (26×51 and 51×101 ; r, ξ)

are used, and no significant differences are seen in the results.

3. RESULTS FOR HORIZONTAL PIPE

3.1. Velocity profiles

The axial variation of velocity profiles along the vertical centerline is shown in Fig. 2. The effect of axial conduction with decreasing Pr on the velocity profiles can be clearly seen in Figs. 2(a)–(d), which correspond to the cases of $Pr = 0.71, 0.1, 0.025$ and 0.001 with $Re = 100$ ($Pe = 71, 10, 2.5$ and 0.1), respectively, at a given Gr of 5000. Generally, the initial parabolic velocity profile is gradually distorted and becomes asymmetric as the maximum velocity displaces toward the bottom pipe wall. In the case of $Pr = 0.71$ ($Pe = 71$) (Fig. 2a), the parabolic profile is maintained in the upstream region except very near the inlet of heating section ($\xi = 0$), where a slight distortion is observed. In the cases of lower Pr , as shown in Figs. 2(b) and (c), the parabolic profile is distinctly distorted in the upstream region and some reverse flow with negative velocity appears near the top pipe wall. When the Prandtl number is much lower at $Pr = 0.001$ ($Pe = 0.1$) (Fig. 2d), asymmetric velocity influenced by free convection occurs far upstream. However, because of the small local temperature difference due to the dominant axial conduction, the distortion of velocity profiles does not become so large. The effect of increasing Gr is seen in Figs. 2(e) and (f), which show the velocity profiles for the cases of $Pr = 0.025$ and 0.007 ($Pe = 2.5$ and 0.7) with a higher Gr of 20 000. Violent reverse flows are observed at far upstream locations, and both free convection and axial conduction effects play a pronounced role simultaneously. Relatively, the distortion of velocity profile in Fig. 2(e) becomes weaker than that in Fig. 2(f) owing to a smaller Pr of 0.007. At far downstream locations, the parabolic profiles reappear with diminishing free convection.

Figure 3 shows the regime of reverse flow occurrence for practical Pe ranging from 0.3 to 10. The occurrence of reverse flow mainly depends on Re and Gr and also slightly on Pr , so the coordinates Pe and Ra are used in Fig. 3. The reverse flow occurs under the condition shown by open symbols. The dashed line (almost linear in the logarithmic coordinates) indicates the limitation of the reverse flow occurrence. As will be discussed later, the occurrence of reverse flow diminishes the heat transfer in low Pe flows, so that Fig. 3 is practically important to predict flow reversal.

The secondary flow velocity vectors at the axial location $\xi = 0.08$ ($x'/r'_0 = 0.145$), very near the inlet of the heating section, are presented in Fig. 4 for $Pr = 0.025$ and 0.001 ($Pe = 2.5$ and 0.1). It is seen that the secondary flow already develops at the location where the heating just begins. In Fig. 4(a), the fluid flows upward along the pipe wall and downward in the central region, since the fluid is warm near

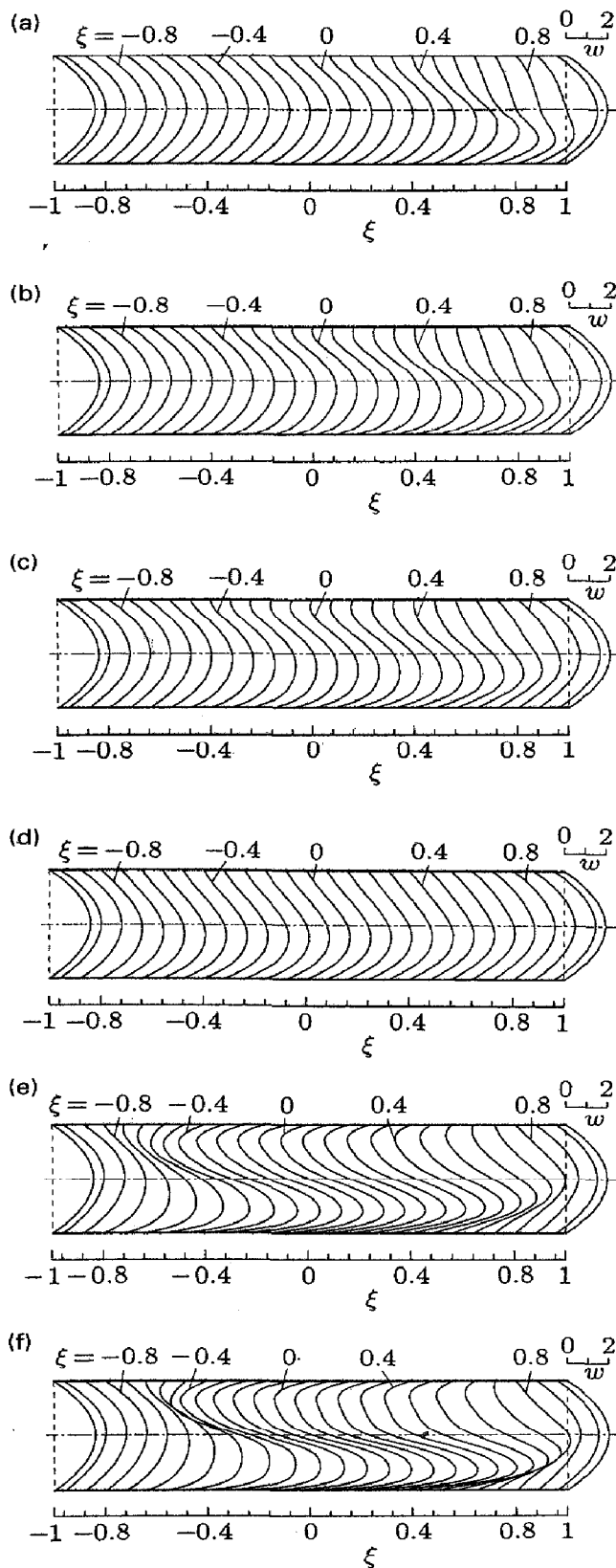


FIG. 2. Velocity profiles along vertical centerline in a horizontal pipe: (a) $Pr = 0.71$ ($Pe = 71$), $Ra = 3550$; (b) $Pr = 0.1$ ($Pe = 10$), $Ra = 500$; (c) $Pr = 0.025$ ($Pe = 2.5$), $Ra = 125$; (d) $Pr = 0.001$ ($Pe = 0.1$), $Ra = 5$; (e) $Pr = 0.007$ ($Pe = 0.7$), $Ra = 140$; (f) $Pr = 0.025$ ($Pe = 2.5$), $Ra = 500$.

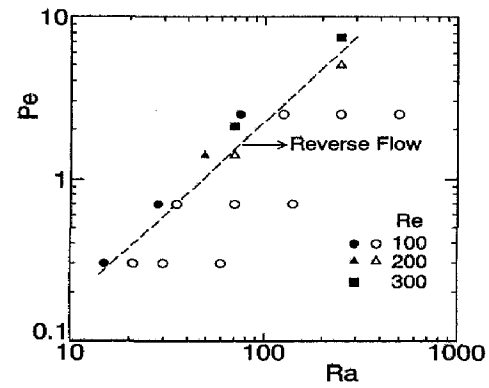


FIG. 3. Regime of reverse flow occurrence for a horizontal pipe.

the wall and cold in the center of the pipe. As the Ra is higher (Fig. 4b), the secondary flow becomes much stronger and more complex. The flow pattern with two vortices in the upper and lower regions of pipe can be observed, in relation to that the reverse flow occurs at the upper region of pipe and the maximum velocity moves toward the bottom pipe wall, as shown in Fig. 2(f). On the other hand, the secondary flow becomes quite weak at very low Pr of 0.001 (Fig. 4c), because of the much smaller difference of local temperature.

3.2. Wall shear stress

The circumferential and axial variations of local wall shear stress are shown in Fig. 5. The dimensionless local shear stress at the wall $\tau_{w\phi}$ is defined by

$$\begin{aligned} \tau_{w\phi} &= -\mu(\partial w'/\partial r')_{r=r_0,\phi}/(\rho w_0'^2/2) \\ &= -(4/Re)(\partial w/\partial r)_{r=1,\phi}. \end{aligned} \quad (21)$$

Since the main flow is forced down toward the pipe bottom by the secondary flow the local wall shear stress varies along the circumferential position with a maximum at the pipe bottom $\phi = \pi$ and a minimum at the pipe top $\phi = 0$. The axial variations of the shear stresses at the bottom and top pipe walls exhibit a peak and a valley. As Pr becomes small the effect of axial conduction reaches far upstream locations and thus the local peak and valley move upstream. With increasing Ra the wall shear stresses at the top and bottom pipe walls show a higher peak and a deeper valley. At $Pr = 0.025$ and 0.007 ($Pe = 2.5$ and 0.7) (Figs. 5b, c), the wall shear stress takes negative values at the top pipe wall due to the occurrence of reverse flow. At far downstream locations, the value of $\tau_w Re = 16$ for the Poiseuille flow is approached as the free convection effect diminishes.

3.3. Temperature profiles

Figures 6(a)–(c) show the axial variation of temperature profiles along the vertical centerline ($\phi = 0$ and π) for the cases of $Pr = 0.71$, 0.025 and 0.001 ($Pe = 71$, 2.5 and 0.1), respectively. In these figures, each of the scales in the coordinate axis

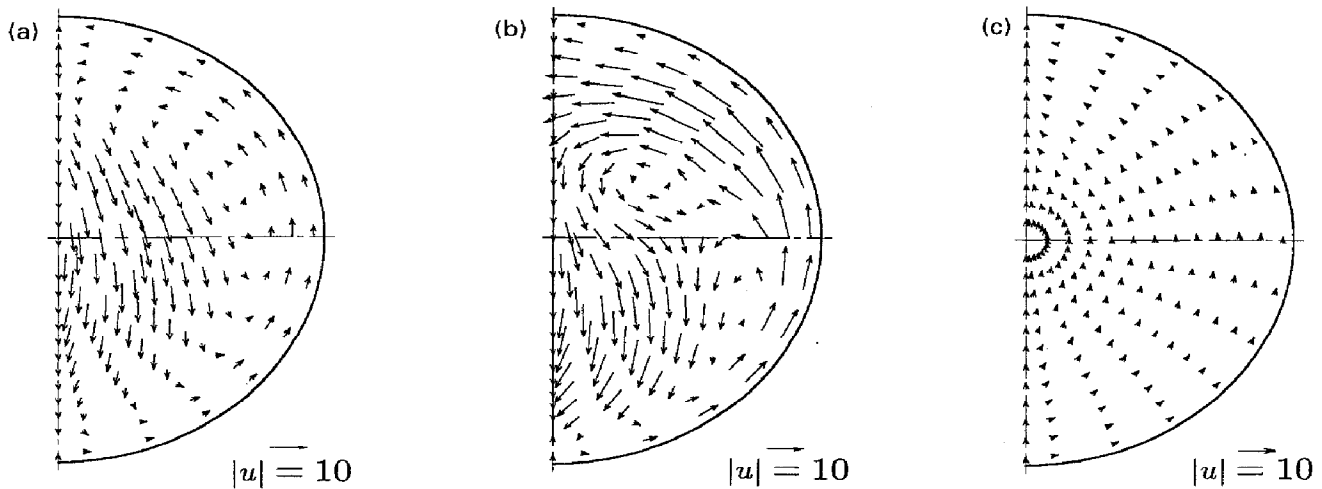


FIG. 4. Secondary flow patterns at $\xi = 0.08$ ($x'/r'_0 = 0.145$) in a horizontal pipe: (a) $Pr = 0.025$ ($Pe = 2.5$), $Ra = 125$; (b) $Pr = 0.025$ ($Pe = 2.5$), $Ra = 500$; (c) $Pr = 0.001$ ($Pe = 0.1$), $Ra = 5$.

ξ stands for a zero point of each temperature profile $(1 - \theta) = (t'_0 - t') / (t'_0 - t'_w)$ at the corresponding location ξ . The effect of Pr on temperature profiles is clearly seen in Fig. 6. In the case of $Pr = 0.71$ ($Pe = 71$) (Fig. 6a), the temperature variation in the upstream region due to the axial conduction effect only appears very near the beginning of heating. The entrance fluid temperature is kept in the pipe core until about $\xi = 0.40$ ($x'/r'_0 = 1.11$). On the other hand, as Pr decreases, the temperature variation in the upstream region becomes larger and extends upstream farther than $\xi = -0.40$ ($x'/r'_0 = -1.11$) and $\xi = -0.64$ ($x'/r'_0 = -2.96$) for $Pr = 0.1$ ($Pe = 10$) and $Pr = 0.025$ ($Pe = 2.5$), respectively, as seen in Figs. 6(b) and (c). In the very low Pr case (Fig. 6e), the fluid temperature begins to vary at a location farther than $\xi = -0.88$ ($x'/r'_0 = -12.22$) owing to the dominant axial conduction effect.

The effect of free convection on temperature profile is also seen in Fig. 6. For Pr from 0.71 to 0.025 (Pe from 71 to 2.5) (Figs. 6a–d), the fluid temperature in the upper pipe region becomes higher and the temperature minimum is shifted toward the pipe bottom, since the warmer fluid near the pipe wall moves upward and the colder fluid in the central region moves downward. Thus, the temperature profile is gradually distorted and becomes asymmetric. In the insulated upstream region, free convection makes the wall temperature at the pipe top higher than that at the pipe bottom. However, such behavior is unnoticeable for $Pe = 0.1$ (Fig. 6e) because the prominent axial conduction weakens the effect of free convection.

The axial velocity contours and isotherms at the location near the beginning of heating, $\xi = 0.08$ ($x'/r'_0 = 0.145$), are depicted in Fig. 7. It is seen that the close similarity between the velocity and temperature profiles existing in the case of air [5] is entirely lost in low Pe flows. The reverse flow region appears near the pipe top at $Pr = 0.025$ ($Pe = 2.5$)

with $Ra = 125$ (Fig. 7a) and extends to about a third of the whole pipe section with increasing Ra (Fig. 7b). Consequently, the velocity of main flow in the lower pipe region increases to conserve the mass flow rate, as already seen in Fig. 2(f). On the other hand, at a very low Pr (Fig. 7c), the temperature profile becomes symmetric and the velocity profile has relatively less asymmetry.

The dimensionless bulk temperature, defined by the following equation, is plotted in Fig. 8, as a function of the dimensionless axial distance for various Pe :

$$\theta_b = \int_0^1 \int_0^{2\pi} \theta wr d\phi dr / \int_0^1 \int_0^{2\pi} wr d\phi dr. \quad (22)$$

It is found that the axial conduction effect is negligible for $Pe > 71$ but becomes important for lower Pe flows. This conclusion fundamentally coincides with that obtained analytically for pure forced convection [13, 14].

The bulk temperature variation in the wide range of axial distance at $Pr = 0.025$ ($Pe = 2.5$) for various Ra is presented in Fig. 9, which shows the relation between free convection and the axial conduction effects. In the far upstream region about $(x'/r'_0)/Pe < -0.4$ ($x'/r'_0 < -1$), the bulk temperature $1 - \theta_b$ becomes higher than that at $Ra = 0$ and increases with increasing Ra . This means that the free convection consequently promotes the axial conduction effect. However, in the region $(x'/r'_0)/Pe > -0.4$, the bulk temperature becomes lower than that in forced flow and weakens the axial conduction effect with increasing Ra , in connection with the occurrence of reverse flow near the top pipe wall.

3.4. Nusselt number

The local Nusselt number is defined by

$$Nu_\phi = 2r'_0 h_\phi / \lambda = -(2/\theta_b) (\partial\theta/\partial r)_{r=1, \phi}. \quad (23)$$

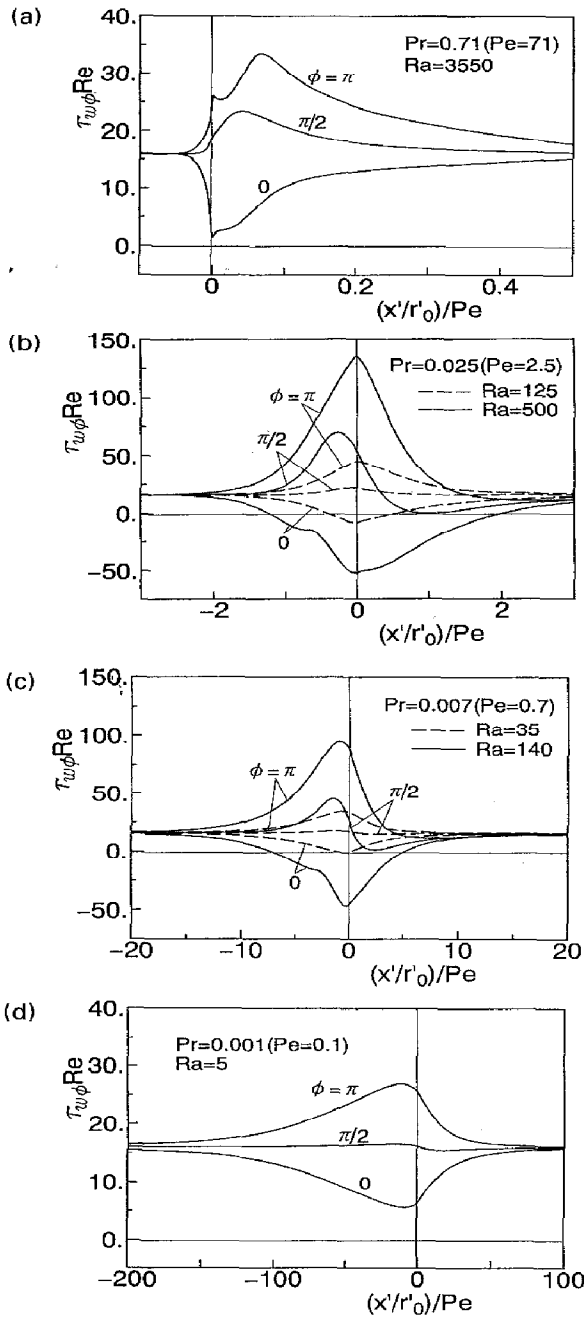


FIG. 5. Variations of local wall shear stress in a horizontal pipe: (a) $Pr = 0.71$ ($Pe = 71$), $Ra = 3550$; (b) $Pr = 0.025$ ($Pe = 2.5$), $Ra = 125, 500$; (c) $Pr = 0.007$ ($Pe = 0.7$), $Ra = 35, 140$; (d) $Pr = 0.001$ ($Pe = 0.1$), $Ra = 5$.

The variation of the local Nusselt-number is shown in Fig. 10 for the cases of $Pr = 0.71$ and 0.025 ($Pe = 71$ and 2.5). For $Pr = 0.71$ ($Pe = 71$) (Fig. 10a), the difference in Nu_ϕ between the top ($\phi = 0$) and bottom ($\phi = \pi$) pipe walls gradually increases with developing secondary flow, and reaches a maximum at the location about $(x'/r'_0)/Pe = 0.07$ ($x'/r'_0 = 5$) where the secondary flow is most intense. For $Pr = 0.025$ ($Pe = 2.5$) (Fig. 10b), however, the difference in Nu_ϕ takes a maximum at the beginning of heating and then decreases monotonously in the downstream direction. As Pr is reduced the effect of axial conduction

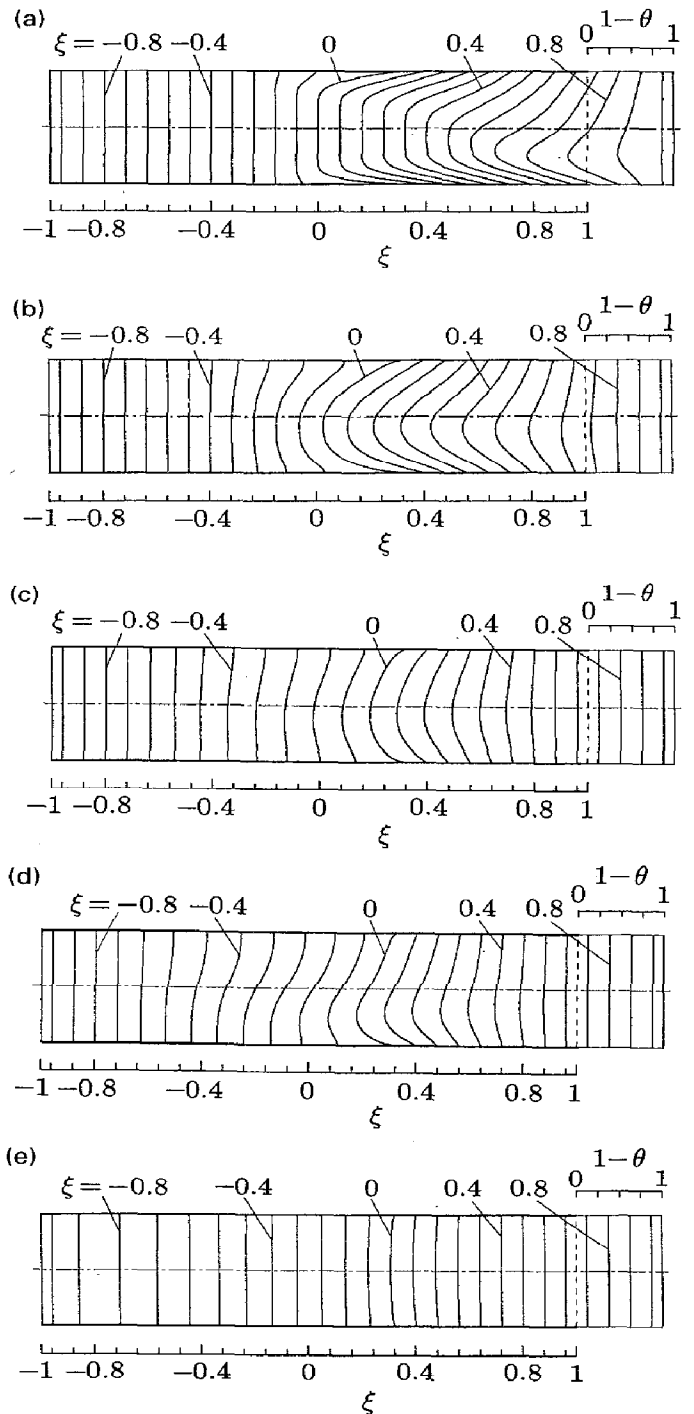


FIG. 6. Temperature profiles along vertical centerline in a horizontal pipe: (a) $Pr = 0.71$ ($Pe = 71$), $Ra = 3550$; (b) $Pr = 0.1$ ($Pe = 10$), $Ra = 500$; (c) $Pr = 0.025$ ($Pe = 2.5$), $Ra = 125$; (d) $Pr = 0.025$ ($Pe = 2.5$), $Ra = 500$; (e) $Pr = 0.001$ ($Pe = 0.1$), $Ra = 5$.

becomes more pronounced and the temperature profile begins to vary in the far upstream region. Consequently, the secondary flow already develops before the fluid enters the heating section and the difference in Nu_ϕ between the top and bottom pipe walls becomes maximum at the heating section inlet.

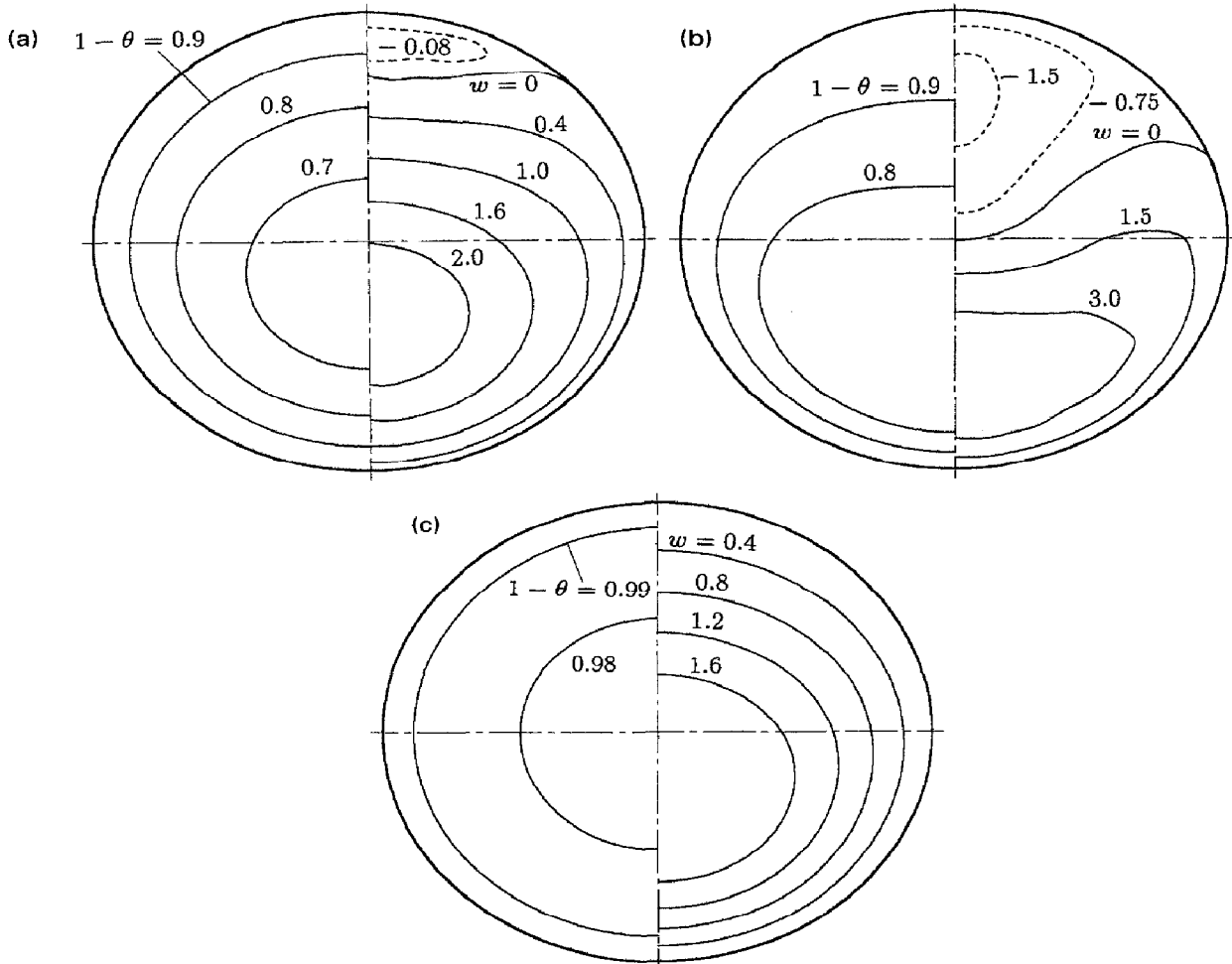


FIG. 7. Axial-velocity contours and isotherms at $\xi = 0.08$ ($x'/r'_0 = 0.145$) in a horizontal pipe: (a) $Pr = 0.025$ ($Pe = 2.5$), $Ra = 125$; (b) $Pr = 0.025$ ($Pe = 2.5$), $Ra = 500$; (c) $Pr = 0.001$ ($Pe = 0.1$), $Ra = 5$.

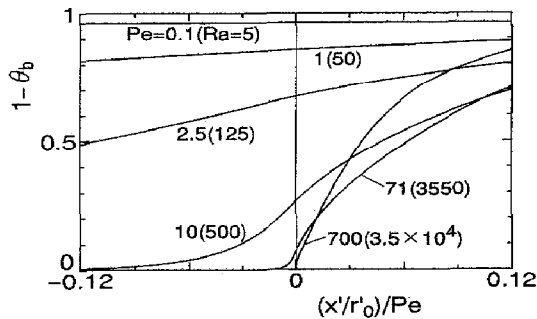


FIG. 8. Bulk temperature variations in a horizontal pipe.

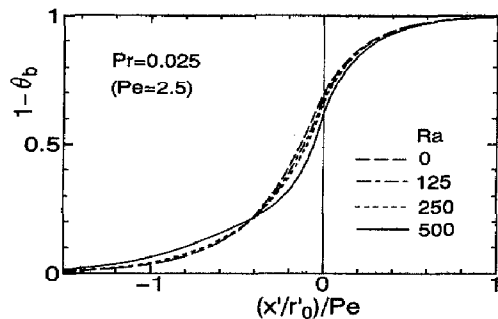


FIG. 9. Bulk temperature variations at $Pr = 0.025$ ($Pe = 2.5$) in a horizontal pipe.

The circumferential average Nusselt number is obtained from

$$\overline{Nu} = \frac{1}{2\pi} \int_0^{2\pi} Nu_\phi d\phi. \quad (24)$$

Figure 11 shows the variations of circumferential average Nusselt number for $Pr = 0.025$, 0.007 and 0.003 ($Pe = 2.5$, 0.7 and 0.3) with various Ra . It is known that the secondary flow occurrence with increasing Ra

enhances the circumferential average Nusselt number for air [5] and larger Pr fluids [6]. For low Pr fluids such as liquid metals, however, the circumferential average Nusselt number tends to decrease with increasing Ra , as seen in Fig. 11. As Ra increases, the secondary flow becomes much more intense and a rather strong reverse flow occurs, so that the fluid temperature rises in the upper region of the pipe and the temperature gradient becomes small at the top pipe wall. Hence, the local Nusselt number Nu_ϕ is

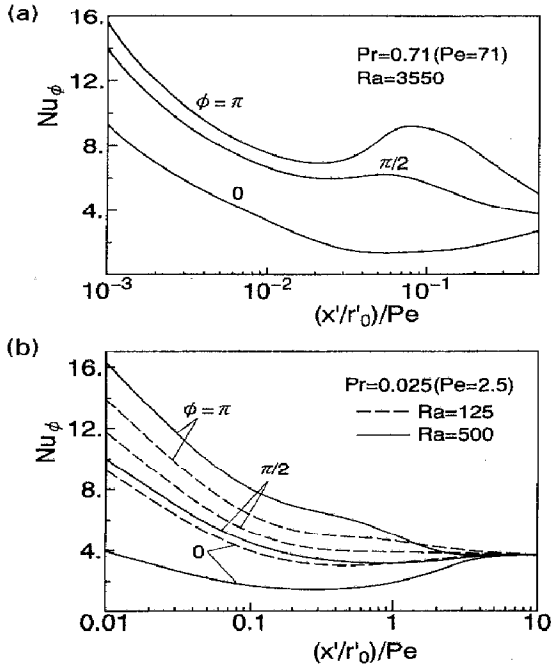


FIG. 10. Local Nusselt number in a horizontal pipe: (a) $Pr = 0.71$ ($Pe = 71$), $Ra = 3550$; (b) $Pr = 0.025$ ($Pe = 2.5$), $Ra = 125, 500$.

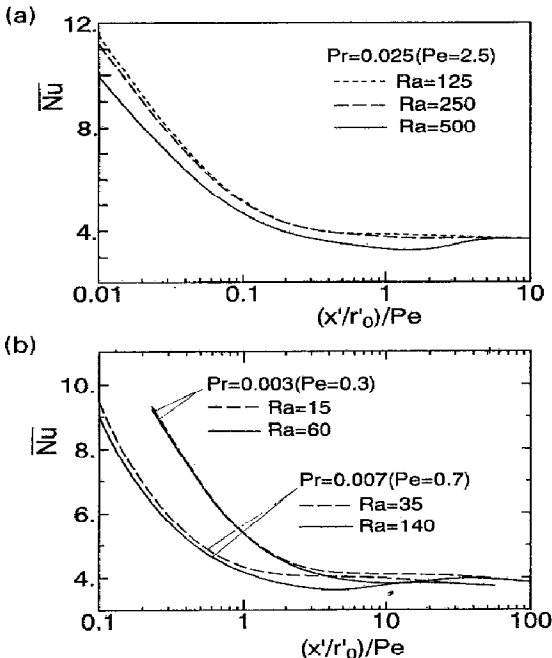


FIG. 11. Circumferential average Nusselt number in a horizontal pipe: (a) $Pr = 0.025$ ($Pe = 2.5$); (b) $Pr = 0.007, 0.003$ ($Pe = 0.7, 0.3$).

reduced extremely at the top pipe wall, and the circumferential average Nusselt number consequently deteriorates. In conclusion, the increase of Ra enhances the circumferential average Nusselt number

for $Pr > 0.1$ ($Pe > 10$) but decreases that for $Pr = 0.003-0.025$ ($Pe = 0.3-2.5$).

Figure 12 shows the axial variations of the circumferential average Nusselt number against various Pe numbers. In the cases of $Pe \geq 10$, the circumferential average Nusselt number takes a local maximum at the location where the secondary flow becomes most intense. After reaching a local maximum, the average Nusselt number decreases until the asymptotic value of $Nu = 3.66$ for the thermally developed flow is approached. The behavior of the average Nusselt number for larger Pe and Ra cases is on the whole the same as that obtained with the large Prandtl number assumption by Ou and Cheng [4]. For $Pe \leq 2.5$, on the other hand, the average Nusselt number decreases monotonously with increasing axial distance, as described above, and approaches the asymptotic value. This asymptotic value depends on Pe and varies from 3.66 for moderate and large Pe to 4.18 for $Pe = 0$, which is in agreement with the analysis of pure forced convection [13].

4. RESULTS FOR VERTICAL PIPE

4.1. Velocity profiles

The axial velocity profiles for the cases of heating and cooling in upward flow are shown in Figs. 13 and 14, respectively. In the heating cases (Fig. 13), the velocity profile is gradually distorted from the parabolic shape and becomes concave, because the fluid temperature near the pipe wall is highest and the fluid velocity accelerates in this region, while the velocity of colder fluid in the pipe core is reduced according to the mass conservation. In the cooling cases (Fig. 14), on the contrary, the profile is distorted with the velocity increase at the pipe center, since the fluid temperature near the pipe wall is lowest and the fluid velocity decelerates in the near-wall region.

In Figs. 13(a) and 14(a) ($Pr = 0.71$ with $|Gr/Re| = 50$), since the axial heat conduction has little effect, the velocity profile keeps the initial shape in the upstream region except for the slight distortion at the location very near the beginning of heating or cooling section. The velocity minimum with a negative value appears at the pipe center in the heating case

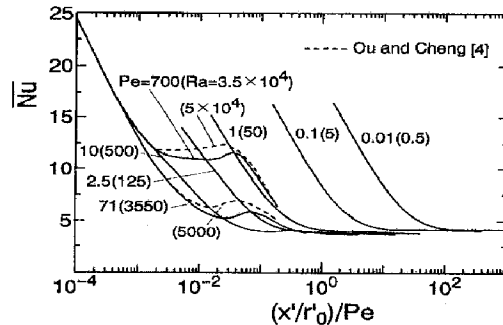


FIG. 12. Circumferential average Nusselt number at $Pe = 700-0.01$ in a horizontal pipe.

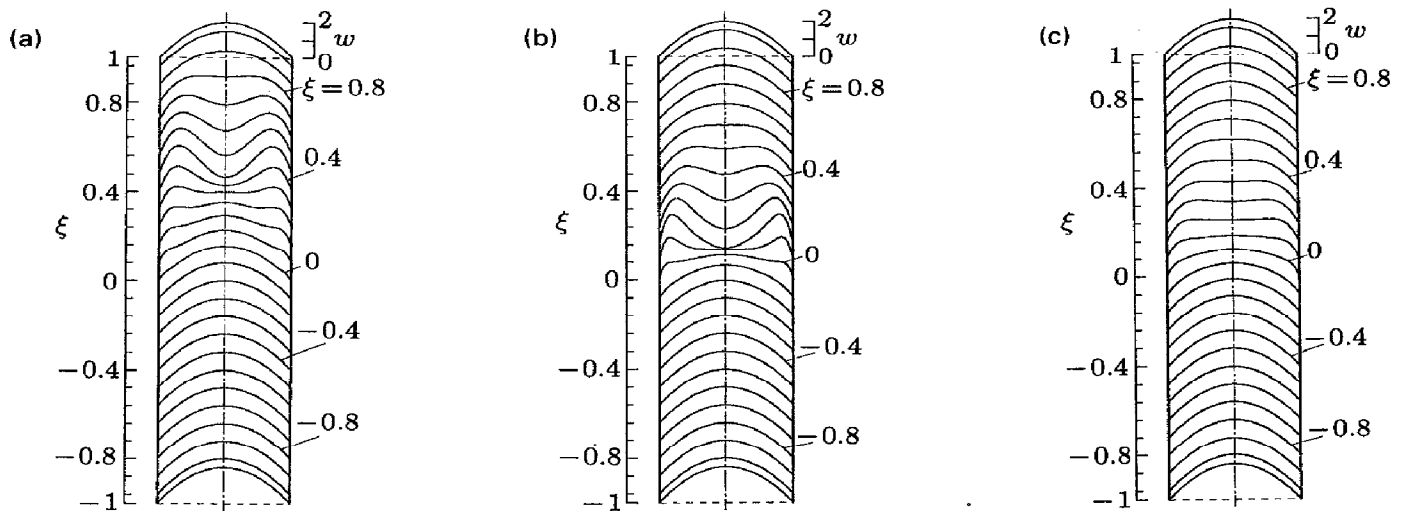


FIG. 13. Velocity profiles for heating cases in a vertical pipe: (a) $Pr = 0.71$ ($Pe = 71$), $Gr/Re = 50$; (b) $Pr = 0.1$ ($Pe = 10$), $Gr/Re = 200$; (c) $Pr = 0.025$ ($Pe = 2.5$), $Gr/Re = 200$.

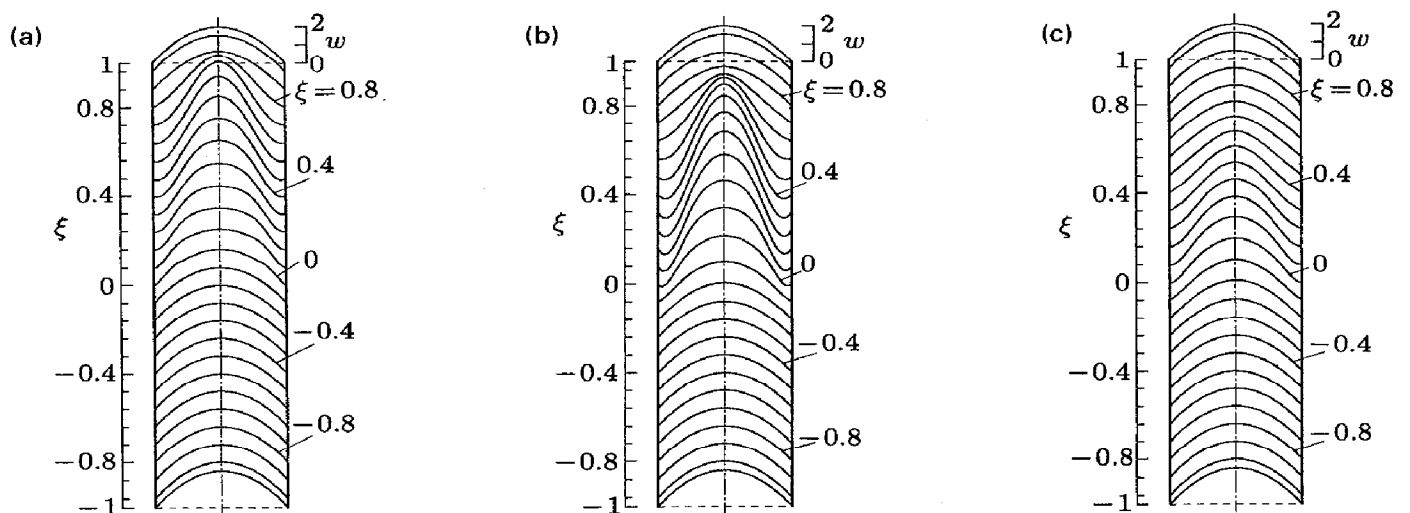


FIG. 14. Velocity profiles for cooling cases in a vertical pipe: (a) $Pr = 0.71$ ($Pe = 71$), $Gr/Re = -50$; (b) $Pr = 0.1$ ($Pe = 10$), $Gr/Re = -200$; (c) $Pr = 0.025$ ($Pe = 2.5$), $Gr/Re = -200$.

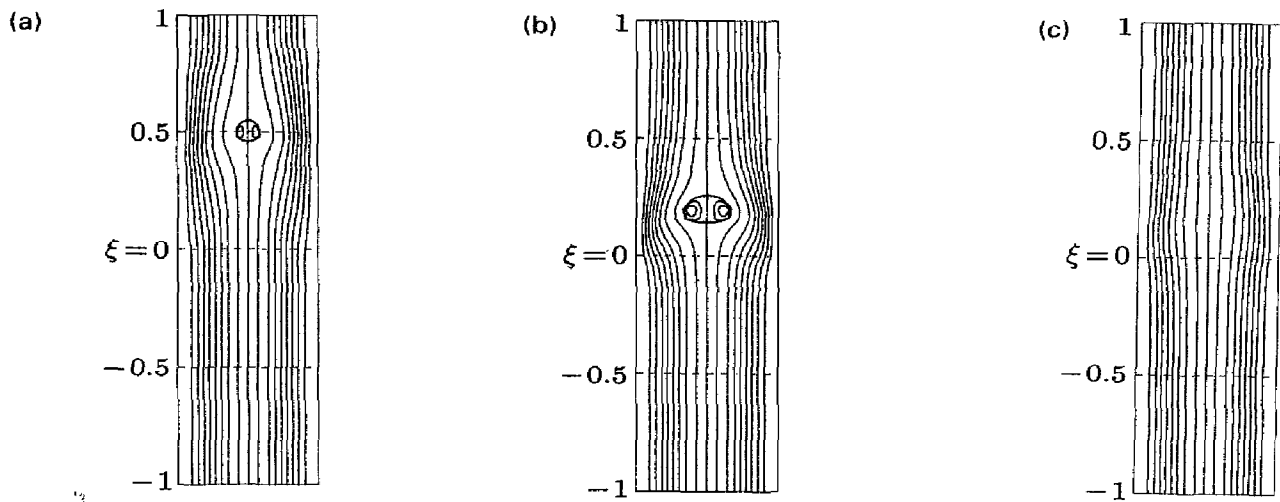


FIG. 15. Streamlines for heating cases in a vertical pipe: (a) $Pr = 0.71$ ($Pe = 71$), $Gr/Re = 50$; (b) $Pr = 0.1$ ($Pe = 10$), $Gr/Re = 200$; (c) $Pr = 0.025$ ($Pe = 2.5$), $Gr/Re = 200$.

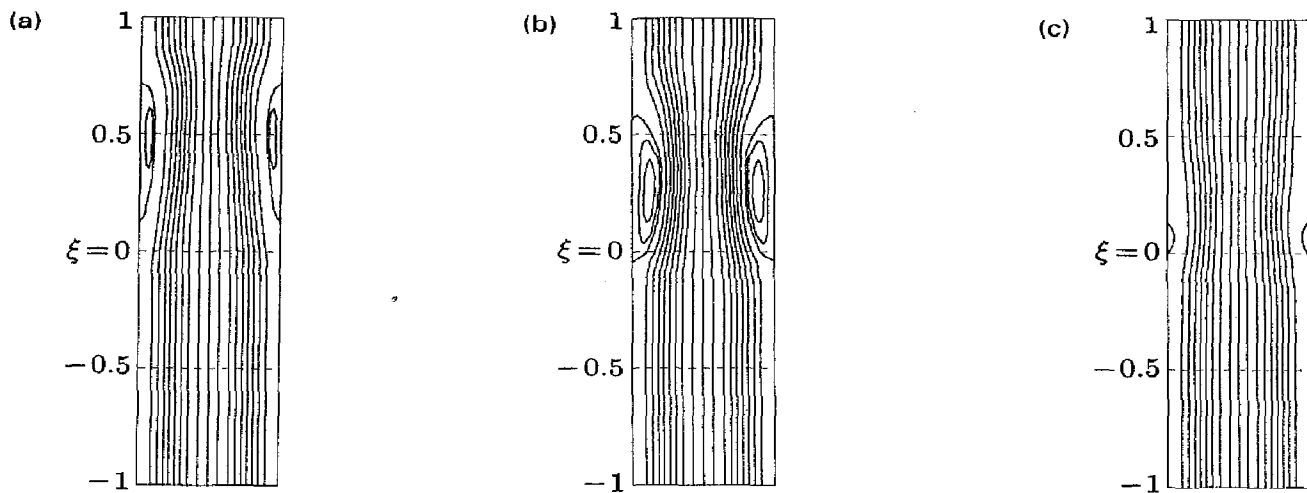


FIG. 16. Streamlines for cooling cases in a vertical pipe: (a) $Pr = 0.71$ ($Pe = 71$), $Gr/Re = -50$; (b) $Pr = 0.1$ ($Pe = 10$), $Gr/Re = -200$; (c) $Pr = 0.025$ ($Pe = 2.5$), $Gr/Re = -200$.

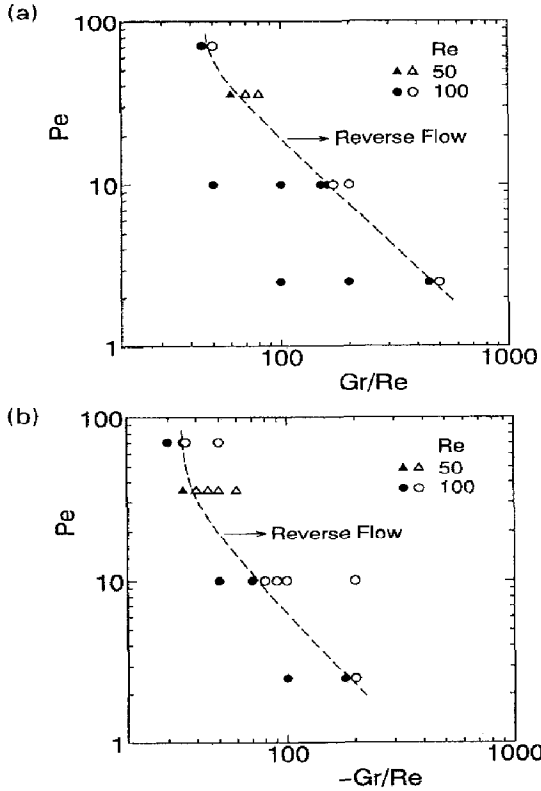


FIG. 17. Regime of reverse flow occurrence for a vertical pipe: (a) heating case; (b) cooling case.

and near the wall in the cooling case, respectively, and a flow reversal is produced. In Figs. 13(b) and 14(b) ($Pr = 0.1$ with $|Gr/Re| = 200$), a strong buoyancy force due to a higher $|Gr/Re|$ results in the marked distortion of velocity profile and extends the flow reversal region. Simultaneously, because the axial conduction effect becomes significant, the velocity profile begins to vary even in the upstream region. The velocity profiles shown in Figs. 13(c) and 14(c) are for $Pr = 0.025$ with $|Gr/Re| = 200$. In either case, the axial conduction has a remarkable effect. However, since the local temperature difference becomes smaller than that in the cases of $Pr = 0.1$ and 0.71 , the distortion of the velocity profile is relatively weak.

Dimensionless streamline plots presented in Figs. 15 and 16 correspond with the heating and the cooling cases shown in Figs. 13 and 14, respectively. The interval of streamlines is mostly 0.06 except in the recirculating region where the streamlines are depicted at an interval of less than 0.06 . These figures clearly show the locations, sizes and shapes of the flow recirculation regions appearing at the center of the pipe in the heating cases (Figs. 15a, b) and in the vicinity of the pipe wall in the cooling cases (Figs. 16a, b). In both heating and cooling cases of $Pr = 0.1$ with $|Gr/Re| = 200$ (Figs. 15b and 16b), quite a strong buoyancy force and relatively significant axial conduction effect play an important role simultaneously, as mentioned before, so that the flow recirculation regions extend and approach the beginning location

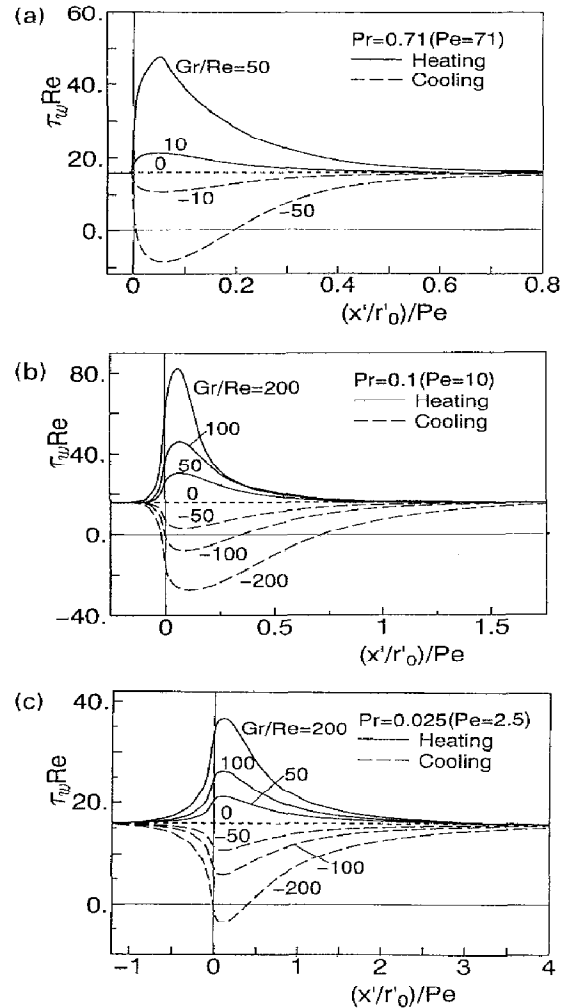


FIG. 18. Variations of local wall shear stress in a vertical pipe: (a) $Pr = 0.71$ ($Pe = 71$); (b) $Pr = 0.1$ ($Pe = 10$); (c) $Pr = 0.025$ ($Pe = 2.5$).

of heating or cooling. In spite of the same values of Pr and $|Gr/Re|$, the flow recirculation region in the heating case is generally smaller and farther from the location of $\xi = 0$ than in the cooling case. This results from the fact that the initial velocity at the pipe center is larger and thus the occurrence of flow reversal in the heating case requires a higher buoyancy force and a longer distance to develop. The streamline plots in Figs. 15(c) and 16(c) correspond with the velocity profiles shown in Figs. 13(c) and 14(c), respectively. The flow reversal is not produced in Fig. 15(c) and just appears in the very small region in Fig. 16(c) because of a relatively weaker buoyancy force. As Pr further decreases to $Pr = 0.007$ with $|Gr/Re| = 200$, the velocity profile shows only a slight distortion and the flow reversal does not occur even at the high $|Gr/Re|$ of 500 .

The regime of the reverse flow occurrence in the coordinates Pe and $|Gr/Re|$ is given in Fig. 17. A reverse flow occurs under the condition positioned in the right-hand side of the dashed line. It is found that for the same Pe the $|Gr/Re|$ value demarcating the

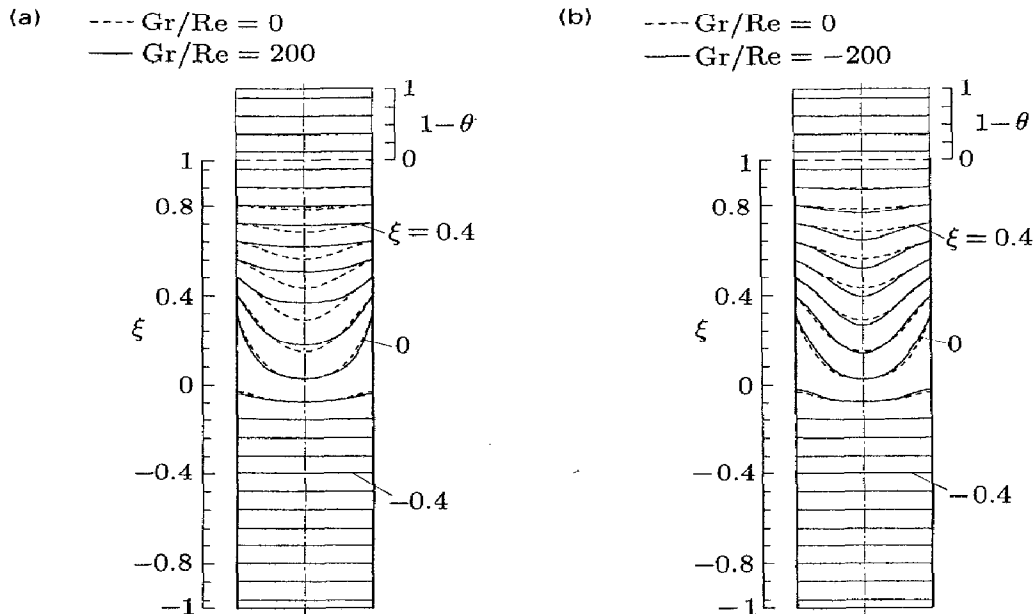


FIG. 19. Temperature profiles for $Pr = 0.1$ ($Pe = 10$) with $|Gr/Re| = 200$ in a vertical pipe: (a) heating case; (b) cooling case.

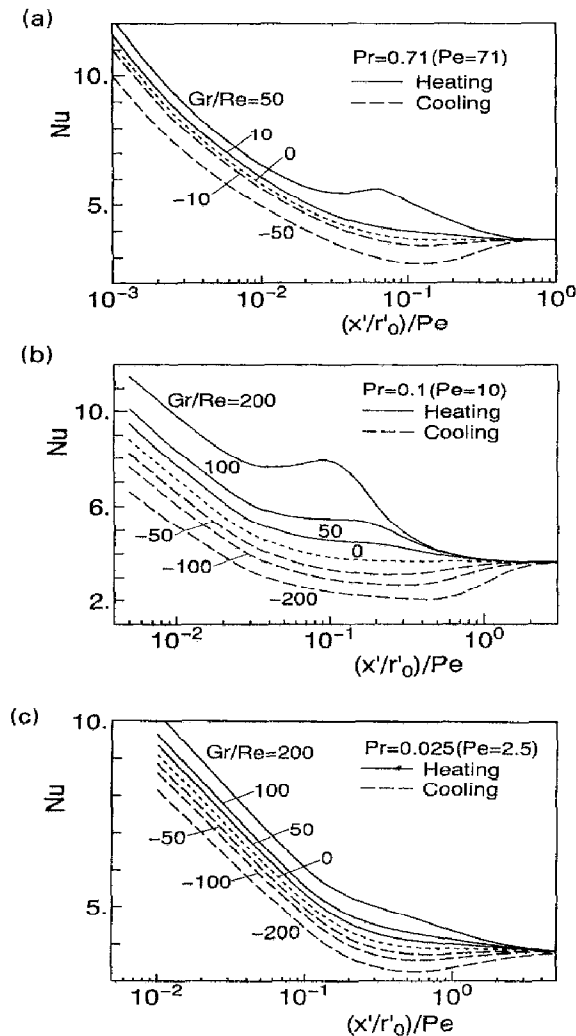


FIG. 20. Nusselt number in a vertical pipe: (a) $Pr = 0.71$ ($Pe = 71$); (b) $Pr = 0.1$ ($Pe = 10$); (c) $Pr = 0.025$ ($Pe = 2.5$).

flow reversal in the heating case is approximately two times that in the cooling case. At $Pe > 50$, the demarcation value tends to approach an asymptotic value independent of Pe .

4.2. Wall shear stress

The wall shear stress distributions with a parameter Gr/Re are presented in Fig. 18 for both heating and cooling cases. The wall shear stress in pure forced flow at $Gr/Re = 0$ takes a constant value ($\tau_w Re = 16$). In the heating cases, since the velocity near the pipe wall accelerates, the wall shear stress increases with increasing Gr/Re . The peaks of τ_w at $Pr = 0.71$ and 0.1 ($Pe = 71$ and 10) occur at the locations where flow reversals begin to appear at the pipe center. In the cooling cases, on the contrary, the wall shear stress becomes smaller due to the deceleration of velocity near the pipe wall and decreases with increasing $|Gr/Re|$. The wall shear stress is negative over the flow reversal region. Additionally, because of the axial conduction, the wall shear stress begins to vary at a far upstream location with decreasing Pr , and the maximum and minimum locations also move toward the upstream. The wall shear stress returns to the asymptotic value of $\tau_w Re = 16$ far downstream, and the distance to the location where the asymptotic value is approached becomes longer in the cooling cases than in the heating cases for low Pr , as seen in Figs. 18(b) and (c).

4.3. Temperature profiles

The temperature profiles at various axial locations in the cases of $Pr = 0.1$ and $|Gr/Re| = 200$ are presented in Fig. 19. In this figure, each of the scales in the coordinate axis ξ stands for a zero point of each temperature profile $(1 - \theta) = (t'_0 - t') / (t'_0 - t'_w)$ at the

corresponding location. It is seen that the temperature profile already begins to vary in the upstream region due to the axial conduction. In comparison with pure forced convection ($Gr/Re = 0$), the temperature in the heating case at $Gr/Re = 200$ becomes higher except in the small region near the beginning of heating. Consequently, the thermal field at $Gr/Re = 200$ develops faster and the heat transfer is enhanced, as will be described presently. On the other hand, in the cooling case, the thermal field at $Gr/Re = -200$ develops more slowly than that of pure forced convection and thus the heat transfer deteriorates, as will be mentioned again later.

4.4. Nusselt number

The Nusselt number distributions with Gr/Re as a parameter are presented in Fig. 20 for both heating and cooling cases. The Nusselt number at $Gr/Re > 0$ (heating case) becomes higher than that at $Gr/Re = 0$ and increases with increasing Gr/Re . In the cases of $Pr = 0.71$ ($Pe = 71$) with $Gr/Re = 50$ and $Pr = 0.1$ ($Pe = 10$) with $Gr/Re = 200$, the Nusselt number takes a local maximum at the location where the flow recirculation occurs. On the other hand, the Nusselt number at $Gr/Re < 0$ (cooling case) becomes lower than that at $Gr/Re = 0$ and decreases with increasing $|Gr/Re|$, taking a minimum before approaching the asymptotic value.

5. CONCLUSIONS

The effects of buoyancy force and axial conduction on the hydrodynamic and thermal characteristics in the thermal entrance regions of horizontal and vertical pipes are investigated numerically for mixed convection at low Pr .

The results obtained for a horizontal pipe are as follows:

1. Distortions of the axial temperature and velocity profiles begin farther upstream due to the effect of axial conduction and free convection with decreasing Pr and become stronger with increasing Ra . Also, the secondary flow develops in the upstream region at low Pr . However, when Pr is extremely low, the effect of free convection becomes rather weak due to the decrease in local temperature difference.

2. The reverse flow with negative velocity is observed near the top pipe wall, and the region where it occurs shifts upstream as Pr becomes low. The occurrence of reverse flow can be identified in the $Pe-Ra$ coordinates.

3. The wall shear stress varies from the minimum at the top pipe wall to the maximum at the bottom pipe wall, and takes negative values at the top pipe wall when the reverse flow occurs. The maximum and minimum positions move toward the far upstream region with decreasing Pe .

4. The local Nusselt number at the top pipe wall decreases extremely with the occurrence of reverse

flow. As a result, the circumferential average Nusselt number also decreases with increasing Ra at low Pr .

The results for a vertical pipe are as follows:

5. The distortion of the axial velocity profiles due to the buoyancy effect becomes larger with increasing $|Gr/Re|$, but weakens considerably at very low Pe flows. Flow reversals are produced at the pipe center in the heating case and near the wall in the cooling case at relatively high $|Gr/Re|$, and the flow reversal regions move upstream due to the axial conduction effect.

6. The occurrence of flow reversal is demarcated in the $Pe-|Gr/Re|$ coordinates, and, if Pe is constant, the demarcation value of $|Gr/Re|$ in the heating case is approximately two times that in the cooling case.

7. The wall shear stress becomes larger in the heating cases but lower in the cooling cases with increasing $|Gr/Re|$. Its maximum or minimum moves toward the point where heat transfer begins as Pe decreases.

8. In the heating case, the Nusselt number increases with increasing Gr/Re and takes a local maximum at a relatively high Pe . In the cooling case, the Nusselt number decreases with increasing $|Gr/Re|$ and reaches its lowest value before attaining the asymptotic value at high Ra .

REFERENCES

1. C. A. Hieber and S. K. Sreenivasan, Mixed convection in an isothermally heated horizontal pipe. *Int. J. Heat Mass Transfer* **17**, 1337–1348 (1974).
2. K. C. Cheng and J. W. Ou, Free convection effects on Graetz problem for large Prandtl number in horizontal tubes with uniform wall heat flux. *Proc. 5th Int. Heat Transfer Conf.*, Tokyo, Vol. 3, pp. 159–163 (1974).
3. S. W. Hong, S. M. Morcos and A. E. Bergles, Analytical and experimental results for combined forced and free laminar convection in horizontal tubes. *Proc. 5th Int. Heat Transfer Conf.*, Tokyo, Vol. 3, pp. 154–158 (1974).
4. J. W. Ou and K. C. Cheng, Natural convection effects on Graetz problem in horizontal isothermal tubes. *Int. J. Heat Mass Transfer* **20**, 953–960 (1977).
5. M. Hishida, Y. Nagano and M. S. Montesclaros, Combined forced and free convection in the entrance region of an isothermally heated horizontal pipe. *Trans ASME, J. Heat Transfer* **104**, 152–159 (1982).
6. F. C. Chou and G. J. Hwang, Numerical analysis of Graetz problem with natural convection in a uniformly heated horizontal tube. *Int. J. Heat Mass Transfer* **31**, 1299–1308 (1988).
7. W. T. Lawrence and J. C. Chato, Heat-transfer effects on the developing laminar flow inside vertical tubes. *Trans ASME, J. Heat Transfer* **88**, 214–222 (1966).
8. W. J. Marnier and H. K. McMillan, Combined free and forced laminar convection in a vertical tube with constant wall temperature. *Trans ASME, J. Heat Transfer* **92**, 559–562 (1970).
9. B. Zeldin and F. W. Schmidt, Developing flow with combined forced-free convection in an isothermal vertical tube. *Trans ASME, J. Heat Transfer* **94**, 211–223 (1972).
10. S. Kieda, T. Chichiki, K. Shimaoka, K. Suzuki and T. Sato, Forced-natural combined heat transfer in the inlet region of a vertical pipe. *Trans Japan Soc. Mech. Engrs* **48(B)**, 1111–1119 (1982).

11. B. R. Morton, D. B. Ingham, D. J. Keen and P. J. Heggs, Recirculating combined convection in laminar pipe flow *Trans ASME, J. Heat Transfer* **111**, 106–113 (1989).
12. D. K. Hennecke, Heat transfer by Hagen–Poiseuille flow in the thermal development region with axial conduction. *Wärme- und Stoffübertragung* **1**, 177–184 (1968).
13. M. L. Michelsen and J. Villadsen, The Graetz problem with axial heat conduction. *Int. J. Heat Mass Transfer* **17**, 1391–1402 (1974).
14. M. N. Özisik, Graetz problems with axial conduction in the fluid. In *Low Reynolds Number Flow Heat Exchangers* (Edited by S. Kakaç *et al.*), pp. 109–135. Hemisphere, Washington, DC (1983).
15. Ş. Bilir, Numerical solution of Graetz problem with axial conduction. *Numer. Heat Transfer, Part A* **21**, 493–500 (1992).
16. T. V. Nguyen, Laminar heat transfer for thermally developing flow in ducts. *Int. J. Heat Mass Transfer* **35**, 1733–1741 (1992).
17. P. J. Roache, *Computational Fluid Dynamics*. Hermosa (1976).